The Astrophysical Journal, 736:109 (13pp), 2011 August 1 doi:10.1088/0004-637X/736/2/109

EJECTA KNOT FLICKERING, MASS ABLATION, AND FRAGMENTATION IN CASSIOPEIA A*

Robert A. Fesen[1], Jordan A. Zastrow[1], Molly C. Hammell[1], J. Michael Shull[2], and Devin W. Silvia[2]
[1] 6127 Wilder Laboratory, Department of Physics & Astronomy, Dartmouth College, Hanover, NH 03755, USA
[2] CASA, Department of Astrophysical and Planetary Science, University of Colorado, Boulder, CO 80309, USA
Received 2011 January 23; accepted 2011 May 3; published 2011 July 14

ABSTRACT

Ejecta knot flickering, ablation tails, and fragmentation are expected signatures associated with the gradual dissolution of high-velocity supernova (SN) ejecta caused by their passage through an inhomogeneous circumstellar medium or interstellar medium (ISM). Such phenomena mark the initial stages of the gradual merger of SN ejecta with and the enrichment of the surrounding ISM. Here we report on an investigation of this process through changes in the optical flux and morphology of several high-velocity ejecta knots located in the outskirts of the young core-collapse SN remnant Cassiopeia A using *Hubble Space Telescope* images. Examination of WFPC2 F675W and combined ACS F625W + F775W images taken between 1999 June and 2004 December of several dozen debris fragments in the remnant's northeast ejecta stream and along the remnant's eastern limb reveal substantial emission variations ("flickering") over timescales as short as nine months. Such widespread and rapid variability indicates knot scale lengths $\simeq 10^{15}$ cm and a highly inhomogeneous surrounding medium. We also identify a small percentage of ejecta knots located all around the remnant's outer periphery which show trailing emissions typically 0.″2–0.″7 in length aligned along the knot's direction of motion suggestive of knot ablation tails. We discuss the nature of these trailing emissions as they pertain to ablation cooling, knot disruption, and fragmentation, and draw comparisons to the emission "strings" seen in η Car. Finally, we identify several tight clusters of small ejecta knots which resemble models of shock-induced fragmentation of larger SN ejecta knots caused by a high-velocity interaction with a lower density ambient medium.

Key words: ISM: individual objects (Cassiopeia A) – ISM: kinematics and dynamics – ISM: supernova remnants

Online-only material: color figure

1. INTRODUCTION

Supernova (SN) ejecta can enrich a galaxy's interstellar medium (ISM) with nucleosynthesis products generated during the progenitor's main-sequence lifetime, post-main-sequence evolution, and the explosive burning that occurs during the SN outburst itself. In this way, SNe influence a galaxy's chemistry by steadily increasing the metallicity of subsequent stellar populations (see Matteucci & Greggio 1986; Pagel 1997; Scalo & Elmegreen 2004; Matteucci et al. 2006; and references therein).

Expanding shells of stellar debris can undergo instabilities leading to the formation of ejecta clumps (Nagasawa et al. 1988; Müller et al. 1991; Kifonidis et al. 2003; Hammer et al. 2010). Indeed, there is considerable observational evidence for ejecta clumping especially in core-collapse SNe (e.g., Filippenko & Sargent 1989; Spyromilio 1991, 1994; Fassia et al. 1998; Matheson et al. 2000; Elmhamdi et al. 2004).

Unfortunately, there are few direct observational constraints regarding the timescales for the fragmentation and dissolution of ejecta clumps as they move through and merge with the progenitor's circumstellar medium (CSM) and local ISM. In contrast to this scarcity of direct observations, the interaction of SN ejecta fragments with local CSM and ISM in supernova remnants (SNRs) has been the subject of many theoretical studies (e.g., Chevalier 1975; Hamilton 1985; Jones et al. 1994; Anderson et al. 1994; Cid-Fernandes et al. 1996; Bykov 2002; Wang & Chevalier 2002). Several related studies have also discussed the properties of the interstellar "bullets" seen in Herbig–Haro (HH) objects and planetary nebulae (Norman & Silk 1979; Poludnenko et al. 2004b; Raga et al. 2007) and there are numerous investigations addressing the general case of a shock wave interacting with interstellar clouds (see Woodward 1976; Stone & Norman 1992; Klein et al. 1994; Mac Low et al. 1994; Pittard et al. 2009, 2010; and references therein).

Young and relatively nearby Galactic SNRs offer the possibility of relatively high-resolution investigations of such SN ejecta ISM/CSM interactions. With the possible exception of the large ejecta clumps seen in the Vela remnant (Aschenbach et al. 1995; Strom et al. 1995; Tsunemi et al. 1999; Katsuda & Tsunemi 2006), the Galactic SNR exhibiting the best example of SN ejecta clumps is the young core-collapse remnant Cassiopeia A (Cas A). With a current estimated age of around 330 years (Thorstensen et al. 2001; Fesen et al. 2006b) Cas A is believed to be the remains of a Type IIb SN event probably from a red supergiant progenitor with an initial mass in the range of 15–25 $M_{\odot}$ which might have lost much of its hydrogen envelope due to a binary interaction (Young et al. 2006; Krause et al. 2008).

Cas A consists of an optical, infrared, and X-ray bright 4′ diameter ($\simeq$4 pc at 3.4 kpc; Reed et al. 1995) emission ring of reverse shock-heated SN debris rich in O, Si, S, Ar, Ca, and Fe (Chevalier & Kirshner 1978, 1979; Douvion et al. 1999; Hughes et al. 2000; Willingale et al. 2002; Hwang & Laming 2003). The remnant's optically visible debris appears as condensations and filaments with typical scale lengths of 0.″2–1.″0 ($(1–5)\times 10^{16}$ cm).

Early broadband photographic images of Cas A taken over several decades starting in the 1950s revealed substantial changes in the brightness and appearance of the remnant's bright main shell of reverse shocked ejecta (Kamper & van den Bergh 1976; van den Bergh & Kamper 1985). These changes have

* Based on observations with the NASA/ESA *Hubble Space Telescope*, obtained at the Space Telescope Science Institute, which is operated by the Association of Universities for Research in Astronomy, Inc.

significantly altered the remnant's overall optical appearance from that seen in 1951 when the remnant was first optically imaged (see van den Bergh & Dodd 1970). Changes in the brightness and appearance of ejecta clumps are fairly gradual, with brightening and fading *e*-folding timescales of around 25 years (Kamper & van den Bergh 1976).

Outside the remnant's main shell of X-ray, optical, and infrared emitting SN debris lie many hundreds of small ($\lesssim$0.″5) optical emission knots with expansion velocities up to 14,000 km s^{-1} (Fesen 2001; Fesen et al. 2006b; Hammell & Fesen 2008). While such outlying ejecta are found around much of Cas A's limb, the majority lie in the nearly opposing northeast (NE) and southwest (SW) ejecta streams or "jets" producing an apparent bipolar asymmetry (Fesen 2001; Hwang et al. 2004; Krause et al. 2005; Fesen et al. 2006a).

To date, no investigation has been made into possible optical flux changes in any of the many hundreds of small ejecta clumps or "knots" lying outside the remnant's main shell. With locations at or ahead of the remnant's forward shock front (Fesen et al. 2006a; Hammell & Fesen 2008), they comprise the vanguard of remnant's SN ejecta and are thus the first to dissolve into and enrich the local ISM. They are not visible due to reverse shock heating as in the main ejecta shell, but are instead shock-heated due to their high-speed passage through the local CSM and ISM.

Here we report results of an imaging survey of some of these outlying debris knots which reveal significant brightness fluctuations over timescales as short as nine months. In addition, a small percentage of knots exhibit trailing emission suggestive of mass stripping and knot disruption due to their high-velocity interaction with local CSM and ISM. We also identify several tight clusters of ejecta knots with a morphology resembling recent model results for the fragmentation of much larger ejecta knots. The observations and knot flux measurement procedures are described in Section 2 with the observational results along with some knot disruption models presented in Section 3 and discussed in Section 4.

2. OBSERVATIONS

Broadband images of the Cas A remnant were obtained using two different cameras on board the *Hubble Space Telescope* (*HST*). Although the primary focus of these images was Cas A's bright main emission shell of SN debris, some of these images cover parts of the remnant's outer periphery, thereby detecting dozens of high-speed outlying ejecta knots.

Four 500 s exposures of the remnant's easternmost limb were taken on 2000 January 23 and 2002 January 16 using the Wide Field Planetary Camera 2 (WFPC2) with the F675W filter. WFPC2 images have an image scale of 0.″1 pixel^{-1} which undersample *HST*'s 0.″046 angular resolution. The F675W filter has a bandpass of 6000–7600 Å and is sensitive to line emissions of [O I] λλ6300, 6364, [N II] λλ6548, 6583, [S II] λλ6716, 6731, [Ar III] λ7136, and [O II] λλ7319, 7330.

Additional WFPC2 images of parts of the remnant's NE jet of ejecta were obtained in 1999 June. These 1999 jet images consisted of four 600 s. Further descriptions of the WFPC2 data and their reduction can be found in Fesen et al. (2001) and Morse et al. (2004).

HST images covering the entire remnant, including all previously known outlying ejecta knots, were obtained on 2004 March 4–6 and 2004 December 4–5 using the Wide-Field Channel (WFC) of the Advanced Camera for Surveys (ACS; Ford et al. 1998; Pavlovsky et al. 2004) on board *HST*. The ACS/WFC consists of two 2048 × 4096 CCDs providing a field of view 202″ × 202″ with an average pixel size of 0.″05. Dithered images were taken in each of the four ACS/WFC Sloan Digital Sky Survey (SDSS) filters, namely F450W, F625W, F775W, and F850LP (i.e., SDSS *g*, *r*, *i*, and *z* filters) to permit cosmic ray removal, coverage of the 2.″5 interchip gap, and to minimize saturation effects of bright stars in the target fields. Total integration times in these filters were 2000 s, 2400 s, 2000 s, and 2000 s, respectively. Further descriptions of these data and their reduction can be found in Fesen et al. (2006a, 2006b) and Hammell & Fesen (2008).

Standard pipeline data reduction of these images was performed using IRAF/STSDAS.[3] This included debiasing, flat-fielding, geometric distortion corrections, photometric calibrations, and cosmic ray and hot pixel removal. The STSDAS drizzle task was also used to combine single exposures in each filter.

For the WFPC2 F675W images, fluxes for eastern limb knots were measured using the IRAF task "apphot." For the ACS F625F, F775W, and F850LP images, calibrated estimates for fluxes of each outer optical ejecta knot for the three filters were taken from the outer ejecta knot catalog of (Hammell & Fesen 2008) which were calculated using the SExtractor (Bertin & Arnouts 1996) automated source extraction software package. For cases where the automated programs failed, knot fluxes were calculated manually five pixel wide apertures. When fluxes were manually calculated, background estimation was performed by calculating the total 5 pixel aperture flux in at least five positions near the object (avoiding other sources) and then subtracting the mean computed "background" flux from the total object pixel sum. Final detector count numbers were then converted to flux by multiplying by the mean flux density per unit wavelength generating 1 count s^{-1} (i.e., the "PHOTFLAM" factor) times the filter effective bandwidth.

Due to the non-spherical nature along with sometimes changing morphology of some ejecta knots, plus the closeness of adjacent emission knots, flux measurements for many of these outlying ejecta knots are subject to greater errors than simply photometric accuracy. Moreover, differences between filter bandpass and system throughputs between the WFPC2 F675W filter and the combined ACS F625W + F775W add to the uncertainty when comparing 2000 and 2002 January WFPC2 fluxes to 2004 March and December ACS fluxes. Nonetheless, since the WFPC2 F675W filter images and the ACS F625W + F775W filter images cover the same ejecta emission lines, namely [O I] λλ6300, 6364, Hα, [N II] λλ6548, 6583, [S II] λλ6716, 6731, and [O II] λλ7319, 7330 (see Fesen 2001 for further details), we have attempted to investigate some knot flux changes over the nearly 5.5 yr interval (1999 June to 2004 December) using these two *HST* image sets.

For our investigation of relative flux differences between different epochs using both WFPC2 and ACS images, detector counts were summed using 5 × 5 to 9 × 9 pixel-sized windows depending on knot size and neighboring emission complexity, subtraction of a local mean background, and finally normalized to the measured flux of several neighboring field stars. Flux errors listed in Tables 1 and 2 include apphot measurement uncertainties, background non-uniformities, and measurement deviations observed when varying knot centroids. While

[3] IRAF is distributed by the National Optical Astronomy Observatory, which is operated by the Association of Universities for Research in Astronomy, Inc. (AURA) under cooperative agreement with the National Science Foundation. The Space Telescope Science Data Analysis System (STSDAS) is distributed by the Space Telescope Science Institute.

Table 1
Observed Fluxes of Selected NE Jet Ejecta Knots

Knot ID	Catalog[a]	F775W[b]		F850LP[b]		2004 Dec/2004 Mar	
(Figure 3)	Number	2004 Mar	2004 Dec	2004 Mar	2004 Dec	F775W	F850LP
1	377	6.4 ± 0.4	20.6 ± 1.3	15.2 ± 0.4	57.8 ± 3.1	3.2 ± 0.4	3.8 ± 0.3
2	381	1.9 ± 0.3	11.7 ± 0.7	5.9 ± 0.6	36.8 ± 2.2	6.2 ± 2.3	6.2 ± 1.2
3	...	1.3 ± 0.3	6.6 ± 0.5	1.6 ± 0.3	7.3 ± 0.4	5.1 ± 2.0	4.6 ± 1.3
4	367	2.5 ± 0.4	9.9 ± 0.5	4.3 ± 0.4	12.7 ± 1.1	4.0 ± 1.0	3.0 ± 0.6
5	...	2.5 ± 0.4	19.3 ± 1.4	5.5 ± 0.5	35.7 ± 2.7	7.7 ± 2.2	6.5 ± 1.2
6	217	5.3 ± 0.3	40.8 ± 1.9	2.3 ± 0.2	11.0 ± 0.5	7.7 ± 0.9	4.8 ± 0.7
7	180	12.8 ± 0.4	5.9 ± 0.5	2.7 ± 0.5	1.7 ± 0.4	0.5 ± 0.1	0.6 ± 0.1
8	581	4.0 ± 0.3	13.5 ± 0.4	11.0 ± 0.7	41.3 ± 2.5	3.4 ± 0.4	3.8 ± 0.5
9	597	3.7 ± 0.3	20.3 ± 0.9	12.0 ± 0.7	63.6 ± 2.6	5.5 ± 0.7	5.3 ± 0.9
10	605	7.2 ± 0.5	3.4 ± 0.3	18.4 ± 0.6	9.6 ± 0.9	0.5 ± 0.1	0.5 ± 0.1
11	713	3.5 ± 0.5	1.9 ± 0.4	7.1 ± 0.7	3.5 ± 0.3	0.5 ± 0.1	0.5 ± 0.1
12	782	1.6 ± 0.3	4.0 ± 0.3	3.3 ± 0.6	8.7 ± 0.5	2.5 ± 0.8	2.6 ± 0.3
13	992	5.9 ± 0.4	16.3 ± 0.7	2.6 ± 0.8	7.1 ± 0.4	2.8 ± 0.3	2.7 ± 0.3
14	914	8.0 ± 0.5	4.1 ± 0.4	8.2 ± 0.5	4.4 ± 0.3	0.5 ± 0.1	0.5 ± 0.1
15	837	6.6 ± 0.5	3.7 ± 0.4	4.8 ± 0.6	3.1 ± 0.3	0.6 ± 0.1	0.6 ± 0.1

Notes.
[a] From the catalog of outer ejecta knots in the Cas A remnant (Hammell & Fesen 2008).
[b] Fluxes are in units of 10^{-17} erg cm^{-2} s^{-1}.

Table 2
Observed Fluxes of Selected Eastern Outer Ejecta Knots

Knot ID	Catalog[a]	2000 Jan[b]	2002 Jan[b]	2004 Mar[c]	2004 Dec[c]
(Figure 5)	Number	WFPC2	WFPC2	ACS	ACS
A	1228	7.3 ± 1.1	9.6 ± 0.7	8.2 ± 0.6	3.5 ± 0.4
B	1273	<1.5	4.4 ± 0.6	4.9 ± 0.5	2.2 ± 0.3
C	1296	5.2 ± 0.7	23.9 ± 1.3	13.1 ± 0.6	5.0 ± 0.5
D	1297	3.2 ± 0.6	2.4 ± 0.7	2.8 ± 0.4	7.6 ± 0.6
E	1323	2.7 ± 0.5	1.5 ± 0.4	5.3 ± 0.3	4.9 ± 0.4
F	1325	4.7 ± 0.5	7.8 ± 0.5	2.4 ± 0.2	2.0 ± 0.3
G	1330	5.5 ± 0.8	12.1 ± 0.6	6.7 ± 0.4	5.1 ± 0.4
H	1344	17.4 ± 2.1	2.7 ± 0.5	4.0 ± 0.2	3.4 ± 0.4

Notes. Fluxes are in units of 10^{-17} erg cm^{-2} s^{-1}.
[a] From the Cas A outer ejecta knot catalog of Hammell & Fesen (2008).
[b] Measured from WFPC2 F675W images.
[c] Measured from combined ACS F625W + F775W images.

most 1σ uncertainties listed are below 10%, measured flux uncertainties can be as much as 30% for some knots.

3. RESULTS

In general, we found that a significant fraction of ejecta knots around all portions of the outer periphery of Cas A show some degree of optical flux variability. Below we discuss these flux changes along with morphological changes in some of these outer ejecta knots. Due to differences in expansion velocities and possible chemical compositions, the following discussion is divided into sections by knot location.

3.1. Northeast Jet Knot Variability

Figure 1 shows *HST* images for one of the streams of ejecta in the remnant's NE jet feature taken at three epochs covering a time span of nearly five years. The top panel is a 1999 June WFPC2 F675W image, the middle panel a 2002 January WFPC F675W image, and the bottom panel a 2004 March F625W + F775W ACS image. All three images are sensitive essentially to the same set of emission lines, namely, [O I] λλ6300, 6364, [O II] λλ7319, 7330, and [S II] λλ6716, 6731. Thus, changes seen between these images should be representative of overall flux changes in a knot's line emission.

As Figure 1 illustrates, large brightness changes occur in many of the NE jet's ejecta knots across the whole length of this ejecta stream during this five-year period. Ejecta knots and knot complexes exhibiting especially large flux increases or decreases have been marked in the figure by circles and boxes, respectively. Despite significant changes in many individual knots and knot clusters, the overall optical appearance of this stream of ejecta does not dramatically change over this nearly five-year time period.

Significant flux changes for some NE jet knots can occur over much shorter timescales and we have investigated whether such changes are associated with varying elemental abundances or changes in the ionization state of the ejecta. To do this, we examined several NE jet ejecta knots using ACS images taken nine months apart (2004 March and December) using the F625W, F775W, and F850LP filters. These filters are primarily sensitive to [S II] λλ6716, 6731, [O II] λλ7319, 7330, and [S III] λλ9069, 9531 line emission, respectively. They thus serve as flux variability indicators sensitive to both knot chemistry and ionization state.

The location of 15 selected knots in the remnant's NE jet which were found to exhibit large brightness changes over this nine-month period are shown in Figure 2, both in relation to the whole remnant and within the NE jet region. Enlargements of the 2004 March and December ACS F625W + F775W images of these 15 knots are shown in Figure 3. To study possible abundance and ionization level changes, we measured F775W (i.e., [O II]) and F850LP (i.e., [S III]) fluxes for 2004 March and December for these knots are listed in Table 1.

Knots that brightened optically over this period are 1–6 and 8, 9, 12, and 13. Conversely, Knots 7, 10, 11, 14, and 15 decreased in flux. Overall, a majority of knot flux changes involved brightening, with only a small percentage of knots showing flux decreases over the 2004 March to December time period. While our investigation concentrated on significant knot flux changes, knots that brightened were found to increase in flux by larger factors (≃3–8) as compared to that seen for knots

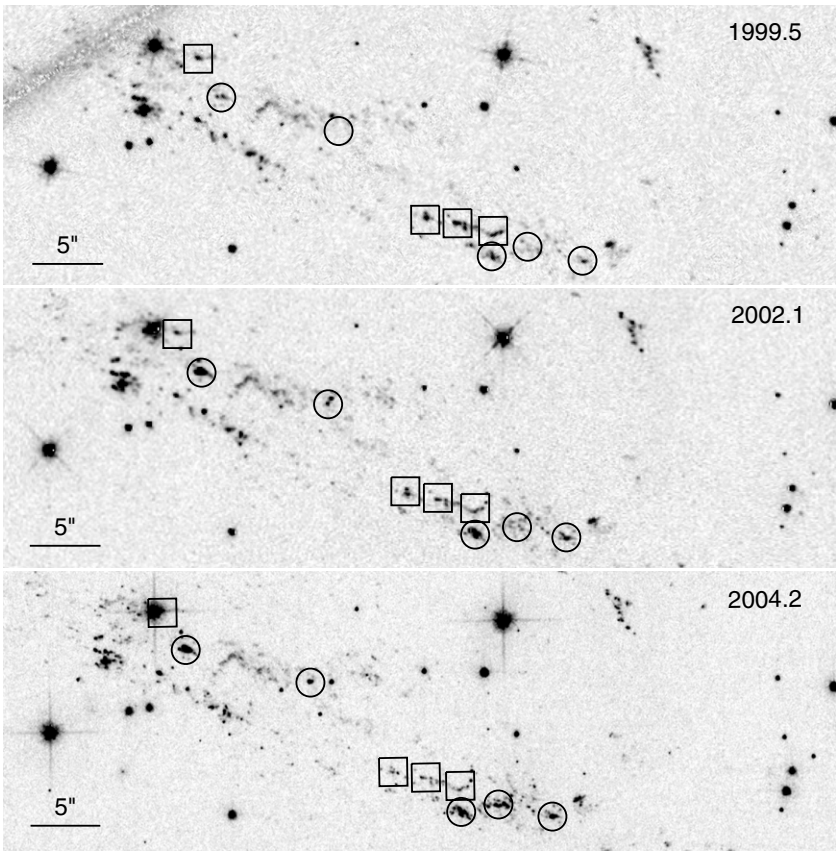

Figure 1. *HST* WFPC2 F675W images (top two panels) and a combined ACS F625W + F775W image (bottom panel) of one of the streams of ejecta knots in Cas A's northeastern "jet" of ejecta. Images cover the time period of 1999.5–2004.2 with a time interval between images of roughly two years. A significant fraction of ejecta knots exhibit changes in brightness, with circles and boxes marking knots showing flux increases or decreases, respectively. The approximate center of field of view of the panels is: α[J2000] = $23^{h}23^{m}49\overset{s}{.}4$, δ[J2000] = $58^{o}49'50''$). North is up, east is to the left.

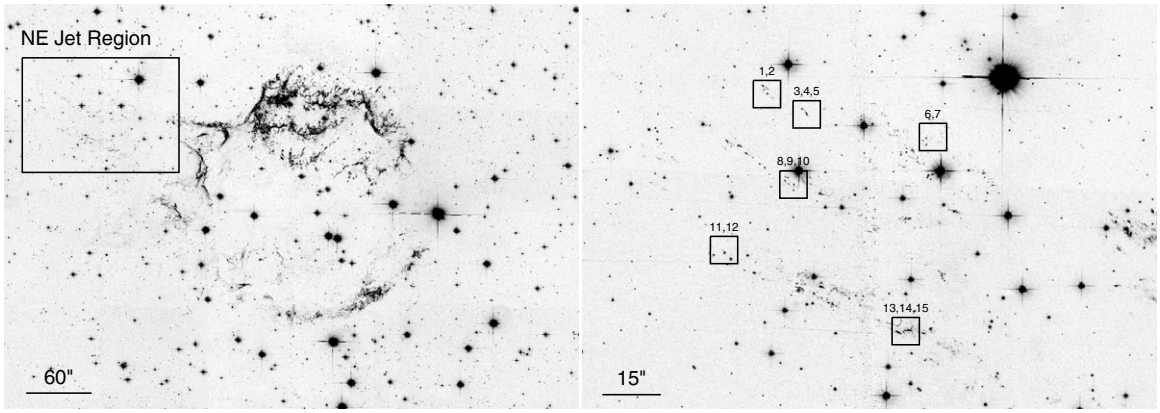

Figure 2. 2004 December *HST* ACS F625W + F775W image of the Cassiopeia A supernova remnant. Left panel marks the area of the remnant's northeastern jet of ejecta knots which is enlarged (right panel) with the six selected areas shown in Figure 3.

that faded. Although the five knots listed in Table 1 which faded between 2004 March and December appear to fade by nearly the same factor of ∼2 suggesting similar decay light curves, examination of other jet knots indicate a wider range of flux decrease is possible. For example, the Hammell & Fesen (2008) catalog Knots 419, 995, and 1019 showed 2004 December/March F775W flux ratios of 0.35, 0.25, and 0.35, respectively.

In general, we detected no pattern in terms of brightness changes between the three filters to suggest systematic changes in the line emissions between knot brightening or fading. This can be seen in Table 1 where we compare the measured F775W and F850LP fluxes which are primarily sensitive to [O II] and [S III], respectively. (Note: we excluded flux measurements in the F625W filter in Table 1 since it is sensitive to both [O I] λλ6300, 6364 and [S II] λλ6716, 6731, thus complicating the interpretation of any observed flux changes.)

While large brightness changes were only seen in a minority of jet emission knots (<25%), smaller flux changes were apparent in a much larger percentage of knots, approaching 50% when viewed over a longer time frame (see Figure 1). However, with few exceptions, faint emission was nearly always visible prior to or following even large brighten or fading episodes

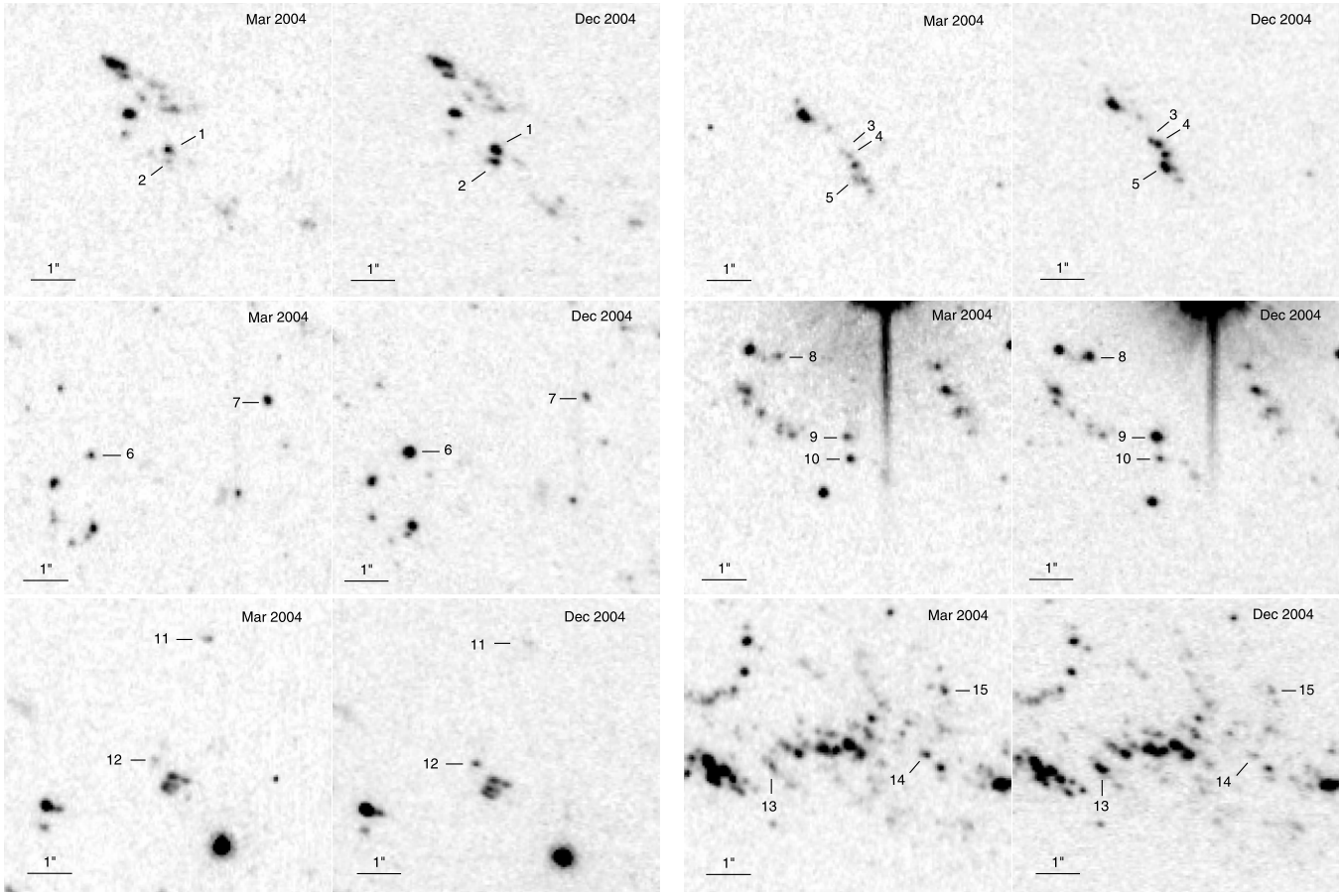

Figure 3. 2004 March and December ACS F625W + F775W images showing flux changes in ejecta knots over a nine-month time span.

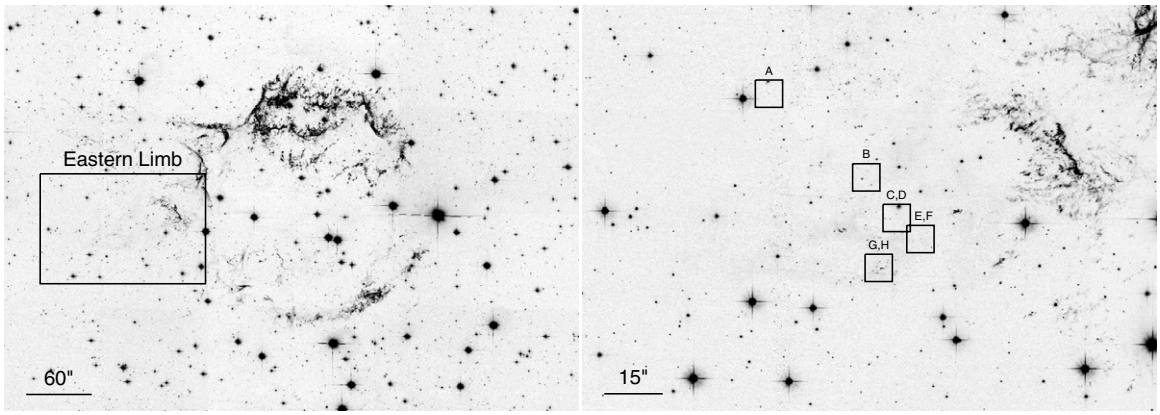

Figure 4. 2004 December *HST* ACS F625W + F775W images of the eastern limb of the Cassiopeia A supernova remnant. Left panel shows the region examined for outer ejecta knot flux variability indicated by the box. The right panel shows the small regions enlarged in Figure 5.

suggesting a minimum excitation level of the ejecta knot outside of these large flux change occurrences.

3.2. Knot Variability along the Eastern Limb

Substantial knot brightness changes were also seen in the remnant's high-velocity ejecta located along its eastern limb. Unlike the NE jet knots, most ejecta here exhibit a spectrum dominated by Hα and [N II] emission lines, indicating a less O- and S-rich composition (Fesen 2001; Hammell & Fesen 2008).

The portion of the eastern limb region that was examined for flux changes is shown in the left panel of Figure 4. Locations of selected ejecta knots showing large brightness changes are marked in the five smaller regions indicated in the right panel of Figure 4, with 2000 and 2002 WFPC2 and 2004 ACS enlargements of these regions presented in Figure 5. Within these smaller regions, flux measurements were made of eight individual knots (Knots A–H; see Table 2).

A variety of light curves was found here, with some knots going up and down in brightness ("flickering") in times as short as one year. For example, Knot A brighten slightly between 2000 and 2002 January but then sharply declined between 2004 March and December (see Figure 5, top row of images). Knot B (second row from top) was undetected in the 2000 January WFPC2 image becoming visible in 2002 January but then faded again

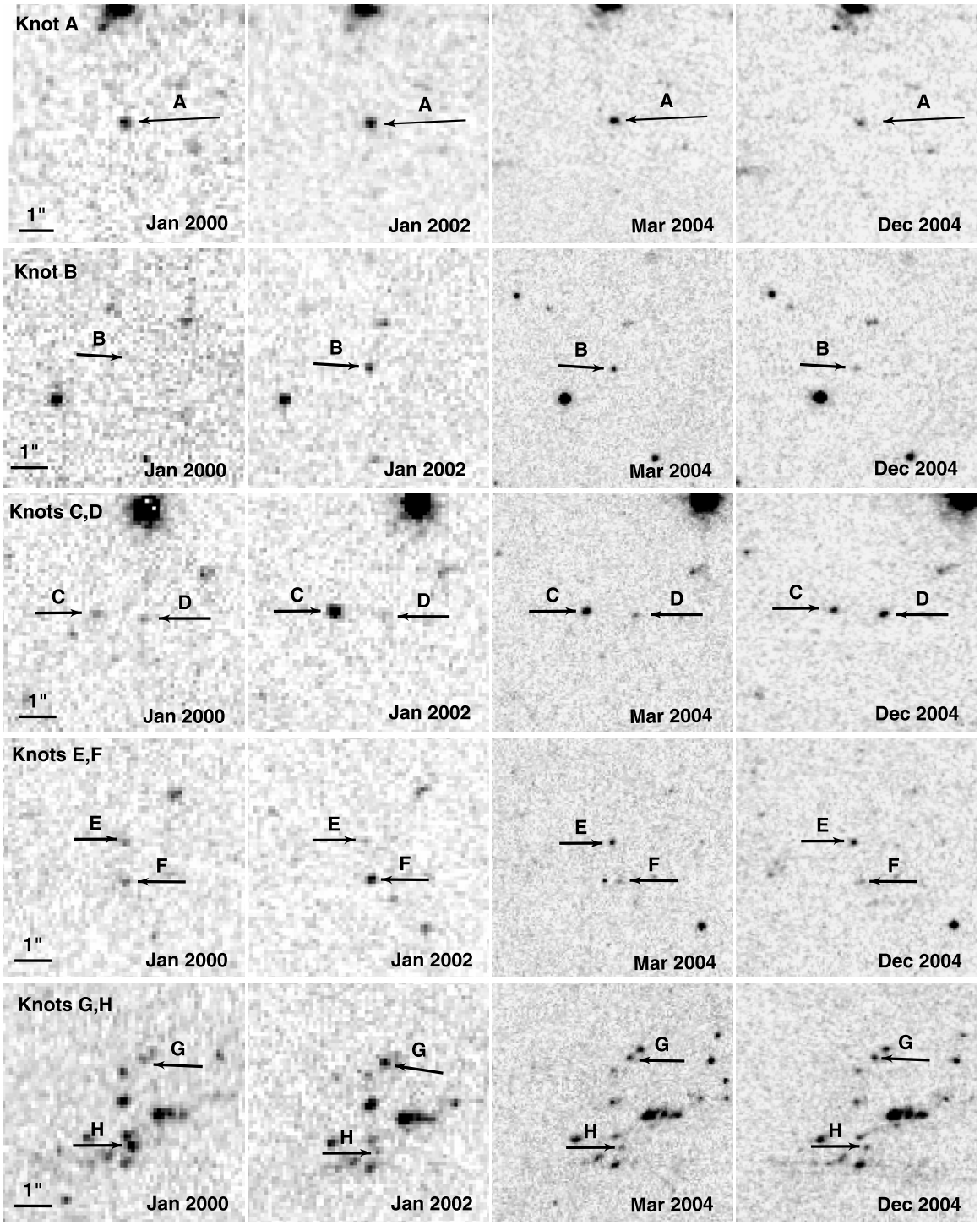

Figure 5. Enlarged 2000 and 2002 WFPC2 images and 2004 ACS images of five regions along Cas A's eastern limb highlighting several SN ejecta knots showing significant flux variations. Measured filter fluxes for knots marked A–G are listed in Table 1.

by 2004 December; whereas Knot G (bottom row) underwent similar flux changes as Knot B, Knot C (middle row) was more extreme, increasing fourfold between 2000 and 2002 but then fading by a similar factor by 2004 December.

In contrast, some ejecta knots such as Knot D were nearly constant in flux (within measurement uncertainties) over nearly four years (2000 January–2004 March) but then showed a substantial brightening over just nine months (2004 March to December). Similarly, Knot F (second row from bottom) showed an abrupt decrease in brightness between 2002 and 2004.

Overall, an array of seemingly random brightness variability, both large and small, was observed not unlike that observed in the NE jet ejecta, except that here we actually observe flickering. While not all outlying eastern limb ejecta knot exhibit large brightness variations over the nearly five-year time frame covered by these *HST* images, many knots did. Increases or decreases in brightness by 25% or more were not uncommon.

Although most brightness changes appear uncoordinated, a few cases do suggest sequential brightening such as the closely spaced Knots C and D (Figure 5, middle row). These two knots

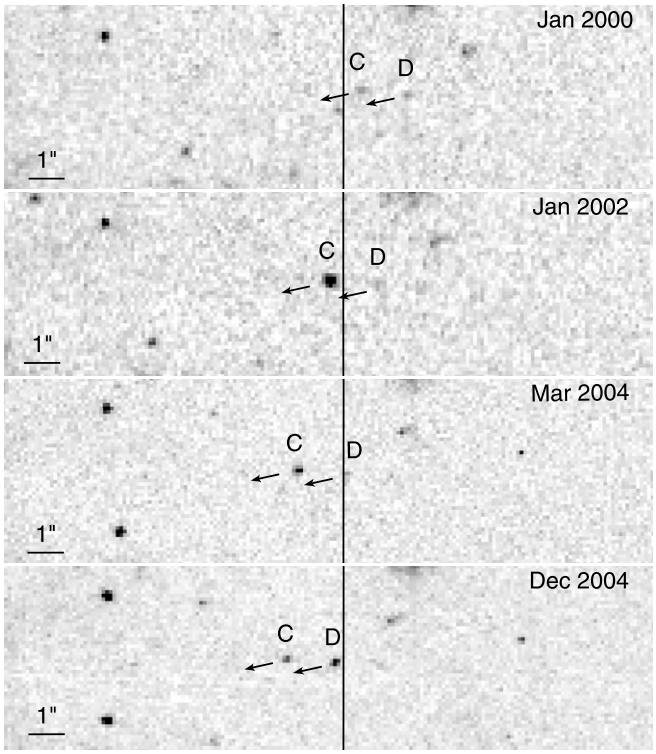

Figure 6. Flux variations of high-velocity eastern limb Knots C and D as they move in the directions indicated by the arrows. The vertical line indicates the location where each knot abruptly brightens, suggestive of an encounter with a circumstellar or interstellar cloud which is invisible in these images. North is up, east is to the left.

are located nearly directly east of the Cas A expansion center with corresponding motions nearly due eastward. As noted above, Knot C significantly brightened between 2000 and 2002 but then sharply faded by 2004 March. Knot D, following closely behind Knot C as seen in projection (separation = 1.″3), showed little change in flux between 2000 and 2004 March but a sharp increase in brightness by 2004 December.

As illustrated by the vertical line shown in Figure 6, the location in the sky were both Knots C and D brightened is nearly the same within 0.″5 suggesting they may have sequentially encountered a circumstellar or interstellar cloud (not visible on these *HST* images) at this spot which led to their shock excitation and hence optical brightening. This is consistent with their observed $1.''3 \pm 0.''1$ separation and their measured proper motion of $0.''434$ yr^{-1} (Hammell & Fesen 2008). These values imply that Knot D would have reached Knot C's projected 2002 January position some three years later and this is exactly what is observed. Knot C brightened in 2002 January roughly three years before Knot D was observed to brighten in 2004 December.

3.3. Knot Emission Tails

The *HST* images of Cas A's outer ejecta knots also revealed a small percentage of knots ($\lesssim$5%) with extended, trailing emission structures or "tails" typically 0.″2–0.″7 in length. Such trailing emission features were found in knots all across the remnant's outer periphery. Figure 7 shows the locations of 10 representative examples of knots with trailing emissions, with enlargements of combined 2004 December ACS F675W + F775W images for these knots presented in Figure 8.

Trailing emissions were always found to be in excellent alignment with the knot's estimated direction of motion strongly

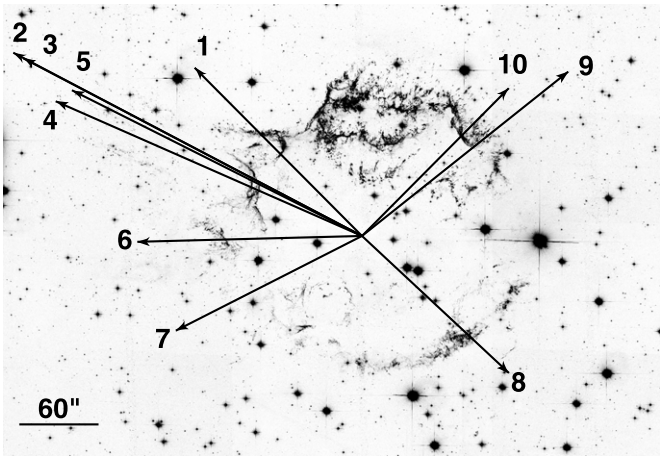

Figure 7. Combined 2004 December *HST* ACS F625W + F775W image of the Cassiopeia supernova remnant. The arrows originate from the remnant's estimated expansion center (Thorstensen et al. 2001) with their tips marking the locations of 10 examples of outlying, high-velocity ejecta knots which appear to exhibit faint trailing emission "tails" as shown in the enlargements presented in Figure 8.

suggestive of mass stripping. This tail–knot motion alignment is illustrated in Figure 8 where each knot is shown twice, with (right panel) and without (left panel) an arrow drawn from the estimated remnant's center of expansion (Thorstensen et al. 2001) out to the knot's 2004 December location. In some cases, the trailing emission appears smooth in intensity away from the knot's head (e.g., Knots 1, 5, 6, and 7), whereas in other cases the trailing emission appears to show one or more trailing emission knots (e.g., Knots 2, 3, and 9).

In principle, these emission tails could be in part or wholly due to shock-excited CSM or ISM emission caused by the passage of these high-velocity ejecta. But this seems unlikely. Comparisons of the knot fluxes in the ACS filters F625W, F775W, and F850LP show no significance difference between a knot's head or its tail in terms of relative strengths. For example, if the tails were due to excited CSM or ISM, Hα and [N II] $\lambda\lambda$6548,6583 would then be expected to be the main emission contributors making the extended trailing emission mainly visible in the F625W images. However, this is not what is observed; trailing emissions are visible in all three filter images consistent with the picture of mass ablation and/or partial knot disruption.

A closer examination of a knot's trailing emission is shown in Figure 9 where we present *HST* image enlargements of a NE jet ejecta knot with a bright emission tail $\simeq$0.″5 long. This knot (#429; Hammell & Fesen 2008) lies in the central region of the NE jet. Intensity plots shown in Figure 10 indicate the trailing emission is some 50%–75% as bright as the knot head itself. In order to generate this level of emission, the material in the tail likely represents a substantial amount of mass.

The length and structure of the knot's trailing emission also change slightly between the March and December images. For example, the knot's emission tail shows the presence of an emission clump in the trailing emission. The clump's position relative to the knot's head changes between March and December in both the F625W and F850LP images amounting to a shift of $\simeq$0.″05 opposite to the knot's outward direction of motion.

The knot has a measured proper motion of $0.''60$ yr^{-1} (Hammell & Fesen 2008) which converts to a transverse velocity of $\simeq$9700 km s^{-1} at a distance of 3.4 kpc. Thus, the smaller forward proper motion of the tail knot implies a lower transverse

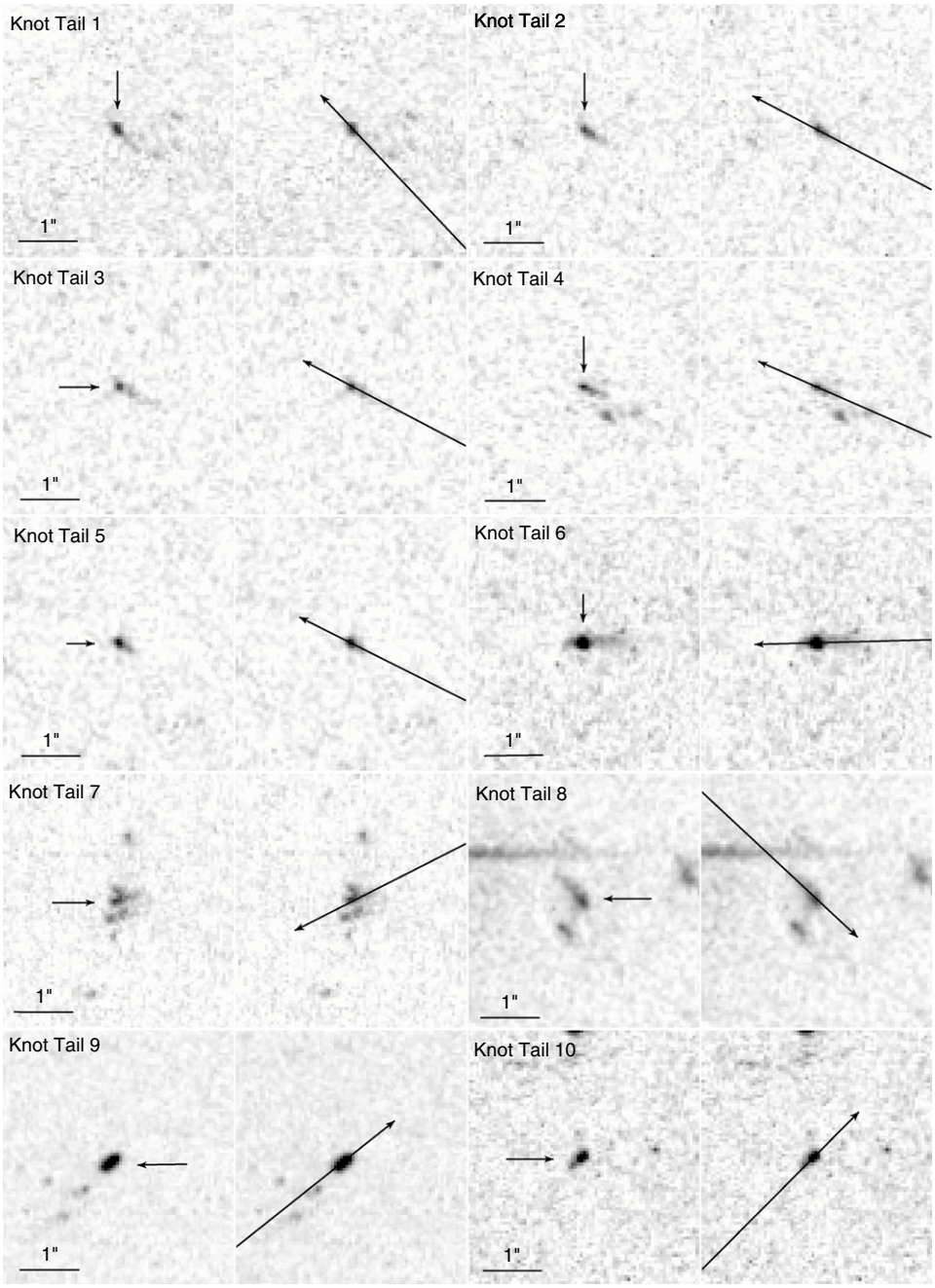

Figure 8. Enlargements of the combined 2004 December ACS F675W + F775W image showing extended emission behind several outlying ejecta knots. Each knot is shown with and without an arrow marking its direction of motion from the remnant's estimated center of expansion.

velocity by $\simeq 800\,\mathrm{km\,s^{-1}}$. This velocity difference, together with it relative brightness, suggests a deceleration of some portion of the main ejecta knot over this nine-month time frame.

4. DISCUSSION

Ejecta knot flickering, ablation tails, and fragmentation are expected phenomena associated with the gradual dissolution of ejecta knots caused by their high-velocity interaction with an inhomogeneous CSM or ISM. In the case of Cas A's outer ejecta whose chemical abundances are significantly non-solar, such changes are subject to very different timescales and scale lengths than seen in other astrophysical settings; e.g., HH objects in T-Tauri outflows.

Several groups have analyzed the dynamical interaction between SN ejecta and a surrounding low-density medium (Chevalier 1975; Hamilton 1985; Jones et al. 1994; Anderson et al. 1994; Cid-Fernandes et al. 1996; Bykov 2002; Wang & Chevalier 2002). A standard feature of this interaction is that a slower shock is driven into the ejecta knot, which subsequently undergoes compression and lateral deformation.

The knot's internal shock heating and subsequent cooling via radiative processes can generate substantial optical line emission. For Cas A's outlying ejecta, the plasma's cooling rate will be enhanced significantly by their metal-rich abundances with additional cooling possible via metal ions sputtered off dust grains (for discussions of dust in Cas A ejecta see Lagage et al. 1996; Arendt et al. 1999; Rho et al. 2008).

The supersonic motion of the knot through the ambient medium will form a bow shock upstream of the cloud and a strong shear layer will develop at the knot's surface which is

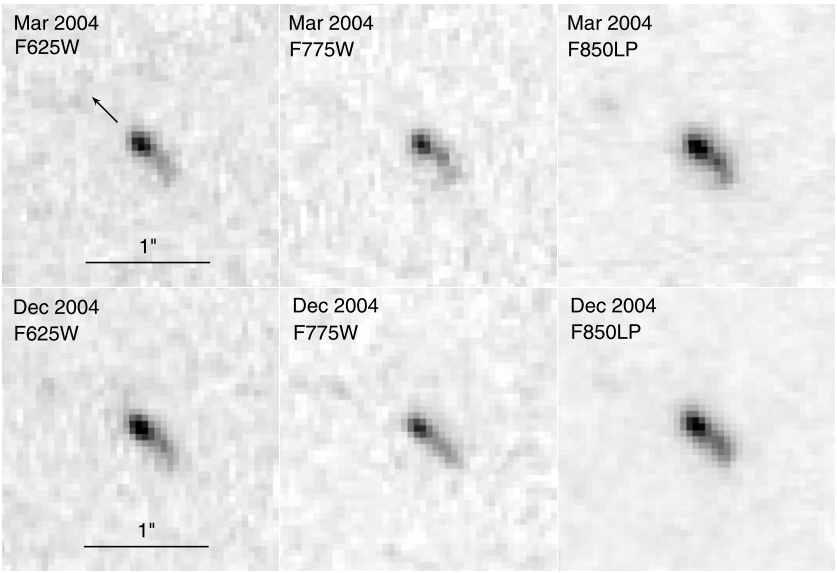

Figure 9. 2004 March and December *HST* ACS F625W, F775W, and F850LP filters images of the ejecta Knot 429 (Hammell & Fesen 2008) in the NE Jet showing a prominent head–tail structure. The arrow in the upper left frame indicates the knot's direction of motion. North is up, east is to the left.

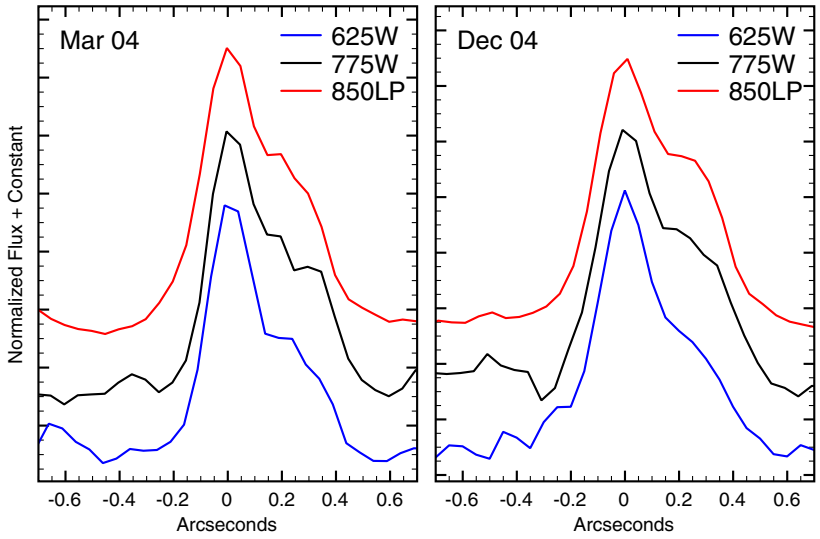

Figure 10. Observed head-to-tail flux plots for the NE Jet ejecta Knot 429 shown in Figure 9.
(A color version of this figure is available in the online journal.)

subject to the Kelvin–Helmholtz instability (Mac Low et al. 1994). The cloud will become compressed by the internal shock with its boundaries distorted by Rayleigh–Taylor and Richtmyer–Meshkov instabilities and by vortex generation as hot gas flows around the knot's edge.

In model simulations of a shocked ISM cloud, a cloud is typically destroyed in several dynamical "cloud-crushing times," t_{cc}, defined as the transit time for the internal shock to move entirely through the knot (Klein et al. 1994; Jones et al. 1994; Poludnenko et al. 2004a). The end result is that the cloud becomes fragmented, decelerated, and eventually shredded.

One can gain some understanding of the relevant timescales for the interaction and microphysical processes with the following estimates. We consider an SNR ejecta knot moving at velocity V_k with respect to the ambient SNR gas, of density $n_e \approx 1$ cm^{-3} (Braun 1987; Chevalier & Oishi 2003; Hwang & Laming 2009). The knot-to-ambient density contrast ratio, χ, typically ranges from 10^2 to 10^4 (Fesen 2001). The internal shock moves through the knot at velocity $V_s \approx \chi^{-1/2} V_k$. Assuming $V_k = 5000$–$10{,}000$ km s^{-1} and $\chi \approx 100$–$10{,}000$, models show the internal shocks propagate at $V_s \approx 100$–500 km s^{-1} (Silvia et al. 2010).

The strong adiabatic shock compresses the gas, initially by a factor of four, and heats the post-shock gas to temperatures between 10^5 K and 10^7 K. The Rankine–Hugoniot temperature jump at the shock front is given by

$$T_s = \frac{3}{16}\left(\frac{\mu V_s^2}{k}\right) = (1.4 \times 10^5 \text{ K})\left(\frac{\mu}{0.6 m_H}\right) V_{100}^2 \qquad (1)$$

for shocks of velocity $V_s = (100 \text{ km s}^{-1}) V_{100}$ and ionized gas with mean molecular weight $\mu \approx 0.6 m_H$.

One can also define the characteristic timescales for knots of transverse size $D = (10^{16} \text{ cm}) D_{16}$ impacted by internal

shocks of velocity V_s and traversing a medium of density $n_e = (10^3\,\mathrm{cm}^{-3})n_3$. As noted above, the internal shocks range from 100 to 500 km s^{-1}, and the observed knot sizes are typically 0.″1–0.″3. At the 3.4 kpc distance estimated for Cas A, an angular size of 0.″1 corresponds to a linear size of 5×10^{15} cm.

The dynamical cloud crossing and gas cooling times are then

$$t_{cc} \equiv D/V_s \approx (30\,\mathrm{yr})D_{16}V_{100}^{-1}$$
$$t_{cool} \equiv \frac{3kT/2}{n\Lambda(T)} \approx (100\,\mathrm{yr})T_6^{1.7}n_3^{-1}Z^{-1}\ . \quad (2)$$

Here, Z is the plasma metallicity in units of solar values, and the radiative cooling function $\Lambda(T) \approx (10^{-22}\ \mathrm{erg\ cm^3\ s^{-1}})T_6^{-0.7}\,(Z/Z_\odot)$. We define the temperature $T = (10^6\,\mathrm{K})T_6$, where the cooling expression is valid over the range $0.3 < T_6 < 10$. At temperatures $1 < T_6 < 10$, the grain sputtering time is fairly constant (Dwek & Arendt 2007),

$$t_{sp} \approx (100\,\mathrm{yr})n_3^{-1}\left(\frac{a}{0.1\,\mu\mathrm{m}}\right) \quad (3)$$

scaled to grains of radius $a \approx 0.1\mu$m. Thus, for temperatures $T_6 \approx 1$ and plasma densities $n \approx 10^3$ cm^{-3}, the grain sputtering time and plasma cooling time are nearly equal and both are comparable to the cloud-crossing time.

4.1. Knot Flux Variability

The basic idea behind emission variations in SN ejecta is that decade-long variability like that seen in the remnant's main shell results from ~100 km s^{-1} shock-wave passage through ejecta knots with characteristic sizes around 10^{16} cm. Smaller knots like those present in the remnant's outskirts and described in this paper allow for faster variability with timescales at or below a few years.

Understanding ejecta knot brightness variability involves both dynamical and radiative processes in the hot post-shock gas. As described by Equations (1) and (2), the characteristic timescales for shock-crossing and radiative cooling of post-shock gas are similar, ranging from 30 to 100 yr for densities $n_e \approx 10^3$ cm^{-3}, knot sizes $D \approx 10^{16}$ cm, and solar metallicities $Z \approx Z_\odot$. Thus the slow, decades-long main shell brightness variations reported by Kamper & van den Bergh (1976) and van den Bergh & Kamper (1985) probably reflect the passage of shocks through large ejecta knots of angular size $\simeq 1''$ (5×10^{16} cm).

Shorter-term ($t \lesssim 1$ yr) variations like those seen in the outer knots involve processes on much smaller scales, as these knots are compressed and fragmented by instabilities arising from the shock passage. Such processes can be seen in the simulations of Mellema et al. (2002), Raga et al. (2007), and Silvia et al. (2010) which show that a shocked cloud with a relatively homogeneous density structure will be dissipated into a cluster of much smaller knots.

Ejecta knots will, if $\lesssim 10^{15}$ cm in size ($\lesssim$0.″02), exhibit optical variability on timescales around 1 yr or less. Thus, the observed rapid shock-induced flux variations on timescales of less than one year suggest significant and dense knot substructures below the diffraction resolution limit of *HST*. However, we will show below in Section 4.3 indications from the lengths of knot emission tails that knot variability is unlikely to be shorter than a few months.

A secondary but important ingredient for creating rapid variability is a highly inhomogeneous ISM or CSM. From a three-year study of infrared light echoes around Cas A, Kim et al. (2008) find that the remnant's local ISM is highly inhomogeneous, consisting of sheets and filaments on a scale of a parsec or less.

However, from our survey of outer knot flux variability, the remnant's circumstellar environment appears to have structures on even smaller scales. For example, the observed flickering of ejecta knots on times of months indicates interactions with small-scale CSM features, as suggested by the rapid flickering of the eastern limb Knots C and D (Figure 6). In that case, the invisible CSM cloud or sheet, which Knots C and D sequentially run into, cannot be much larger than 0.″5 or about 0.01 pc.

It is important to note that our investigation into rapid ejecta knot flux variations was limited by the shortest time interval between images, namely the nine-month separation of the 2004 ACS images. Since it is unlikely that these images captured a knot either at its maximum or its minimum flux brightness, the optical flux variations illustrated in Figures 1–6 and tabulated in Tables 1 and 2 may not necessarily represent the shortest times by which knots substantially brighten or fade. For example, an ejecta knot could have brightened earlier than 2004 March and then begun to fade during our nine-month observing period, meaning that our measured flux variation represents only a minimum change in flux. Similarly, if a knot brightened slowly, then our observed flux change is again a minimum value. Larger flux changes over longer timescales are, in fact, suggested by the sudden appearance of knots in both the jet and eastern limb regions.

4.2. Knot Deceleration

A knot will undergo deceleration both from the direct interaction with local gas as well as from the internal shock driven into the knot that gives rise to the optical emission observed (Jones et al. 1994). If individual ejecta fragments are treated as dense undistorted knots, then their deceleration due to drag from its interaction with the ambient medium depends on the knot's velocity and mass, the density of the local medium, and the cross-sectional area of the knot's bow shock, which for hypersonic conditions is approximately equal to the knot itself (Chevalier 1975; Hamilton 1985; Jones et al. 1994).

The timescale for knot deceleration (drag) is given by $\tau_{drag} \sim \chi R_k/V_k$, where χ again is the density contrast between the knot and the ambient medium (i.e., ρ_k/ρ_a), R_k is the knot's radius, and V_k is the knot's velocity (Jones et al. 1994). Based on ACS imaging data, typical outer knots have velocities of 10,000 km s^{-1} and diameters $\simeq$0.″1 to $\simeq$0.″3 corresponding to $\simeq 1 \times 10^{16}$ cm at 3.4 kpc (Hammell & Fesen 2008). High-velocity outlying [S II] emitting knots exhibit electron densities lie between 2000 and 16,000 cm^{-3} with typical values between 4000 and 10,000 cm^{-3} (Fesen & Gunderson 1996; Fesen 2001).

Choosing $\chi = 10^4$ and an outer ejecta knot velocity of 10,000 km s^{-1} leads to $\tau_{drag} \sim 2000$ yr, suggesting that outer knot deceleration due to drag may be fairly small. However, if the knot fragments into smaller knots as some models suggest (Raga et al. 2007; Silvia et al. 2010), smaller knots will decelerate more rapidly owing to their larger surface area-to-mass ratios. A significant deceleration of cloud fragments would be consistent with observed lumps in the ablation tails of some ejecta knots like that shown in Figures 8 and 9.

4.3. Knot Ablation Tails

Cloud–ISM interaction models suggest knot disruption might also occur due to Rayleigh–Taylor and Kelvin–Helmholtz instabilities resulting in both mass ablation tails as we observed in

some knots and the generation of smaller, dense knot fragments (Klein et al. 1994; Jones et al. 1994; Cid-Fernandes et al. 1996; Raga et al. 2007; Silvia et al. 2010). The timescale for initial knot breakup under these conditions, $\tau_{\rm break}$, is uncertain but is likely to be a few cloud crushing times or $\tau_{\rm break} \sim 4\ \chi^{1/2} R_k/V_k$.

Model calculations by Poludnenko et al. (2004a) for a dense knot moving at 235 km s^{-1} in a relatively dense medium but of similar size to the outer ejecta seen in Cas A showed that deceleration of some of a knot's mass due to fragmentation of the knot will result in a Hubble-like flow of ablated and stripped material flowing off the knot. The fact that most trailing emission tails we observed in Cas A are relatively bright and sometimes clumpy suggest significant mass stripping and partial knot breakup. A possible example of knot fragmentation is Knot 9 (see Figure 8) where the knot appears noticeably elongated in its direction of motion with a possibly associated fainter knot some 0.″6 behind which itself has some trailing emission.

The length of an observed ablation tail is limited by the decline in emission measure (EM $= n_e^2\, L$) as the hot post-shock gas expands and cools. Because this stripped material may form a fairly a continuous medium of gas with similar velocities and densities detached from the main knot, tail material will not experience a strong internal shock. Thus, trailing material should fade in brightness in a timescale roughly equal to the material's post-shock cooling timescale. This can be estimated from the previous sections regarding knot variability and these data suggest a timescale for substantial fading on the order of several months. Such a timescale is consistent with the observed length of knot emission tails. For example, proper motions of Cas A's outer knots are $\sim$ 0.″4–0.″9 yr^{-1} (Hammell & Fesen 2008) meaning that a typical outer knot will move an angular distance roughly 0.″2–0.″5 in a time span of $\sim$0.5 yr, during which time its trailing ablated material cools and hence fades. This agrees well with what is observed.

Presumably all optical visible ejecta knots undergo some degree of mass loss due to shock instabilities on the front and sides of the ejecta knot. However, only a relatively small percentage ($\leqslant$5%) of outer ejecta appear to have visible ablation tails on broadband *HST* ACS images. Poludnenko et al. (2004b) found that knot fragmentation was key in producing significant wake emission. To investigate the formation of visible emission tails, we ran a series of model calculations similar to those presented in Silvia et al. (2010) but where a knot of initial density 1000 cm^{-3} and temperature of 10^4 K and an oxygen abundance 100 times solar passed through a medium of density of 1 cm^{-3} with a velocity of 10,000 km s^{-1}. Under such conditions, a substantial tail in terms of emission measure was formed. Our simulations also showed that with $\chi \sim 100$, the knot was disrupted too quickly to show a strong head–tail structure, whereas if $\chi \gg 10^4$ then too little material was ablated in a trailing wake to be readily visible.

Prior model simulations of small knots have suggested that the inevitable instabilities associated with shock heating are likely to have short lifetimes on the order of t_{cc} (Jones et al. 1994), which for a 0.″2 diameter knot with an internal shock velocity $\simeq$100 km s^{-1} is about 30 yr. This time frame is consistent with observations of the brighter of Cas A's outer ejecta knots which have been bright enough to be optically visible for several decades and some of these show emission tails in *HST* images. One example is the trailing emission Knot 9 shown in Figure 8 (referred to as Knot 10 in Fesen 2001) which is visible on a deep red 1976 Palomar 5 m photographic plate (PH 7252vb: 098-04 emulsion + RG645 filter; van den Bergh & Kamper 1983). Thus this knot, which exhibits very weak Hα emission but strong [N II] emission lines, has been optically bright for nearly three decades (Fesen 2001).

Finally, we note that the emission tails seen for Cas A's outer ejecta knots appear morphologically different from the emission spikes or "strings" seen emanating from the η Carinae Homunculus nebula (Meaburn et al. 1987, 1996; Morse et al. 1998; Weis et al. 1999). These long (4″–16″) and thin (0.″1–0.″25) emission features are thought to be decelerated ablated mass loss caused by the motion of $\sim$1000 km s^{-1} "bullets" of ejected material moving through the star's surrounding CSM (Redman et al. 2002; Currie 2003; Poludnenko et al. 2004a).

Unlike the trailing emission features seen in Cas A, however, the five η Carinae strings are not perfectly straight, they seem to fade in brightness with increasing distance from η Carinae and show no obvious optical emission "head" or leading knot of emission. These properties are quite unlike what is observed in the trailing ablation flows associated with Cas A's ejecta knots.

The lack of an obvious knot at the tip of any of these emission strings has been attributed to very high post-shock temperatures ($\gtrsim 10^6$ K) initially present in the ablated material making them appear weak optically (Redman et al. 2002; Poludnenko et al. 2004a). Interestingly, exactly the reverse is observed in Cas A where we see emission directly attached to the hypersonic knots which have expansion velocities an order of magnitude greater that seen in η Carinae.

We speculate that the emission strings seen in η Carinae represent ablation flows in which ejected knots are largely destroyed and dissolved by their passage through the relatively dense CSM around η Carinae. This would account for both the fading of the strings with increasing distance and the lack of any observable optical bullet head at the string tips.

4.4. Ejecta Fragmentation

Besides the noted clumpiness of some emission tails, there are additional indicators for the disruption and fragmentation of ejecta knots, in particular the breakup of relatively large ones. The evidence comes from the presence of several unusually tight clusters of ejecta knots present in the remnant's NE jet. These clusters consist of several closely spaced knots of similar size and brightness. Four examples of such knot clusters present in the NE jet are shown in the upper panels of Figure 11.

Morphologically, these tight knot clusters appear similar to the results of shock models which show the fragmentation of a large ejecta knot into a tight cluster of small, denser knots (Mellema et al. 2002; Raga et al. 2007; Silvia et al. 2010). To illustrate this, we show in the lower panel of Figure 11 the model results from Silvia et al. (2010) for the evolution of ejecta into a knot cluster over a time span of a few cloud-crushing timescales. Although the jet knot clusters are aspherical and hence look different morphologically from the spherical knot clusters seen in the model results, the exact structure knot clusters will of course depend upon the initial size and structure of the ejecta cloud prior to shock passage and is unlikely to be spherical.

Other examples of small clusters of ejecta knots are two ejecta knot clusters situated along the remnant's northern periphery. Although initially thought to be two single knots from inspection of ground-based images (knots 15 and 15A; see Fesen 2001), *HST* images resolve them into two tight groups of knots each consisting of a dozen or so individual knots (see on-line Figure Sets 2 & 3 for Region H; Hammell & Fesen 2008). The outlying Knot 15 (also known as Knot 91, Kamper & van den Bergh

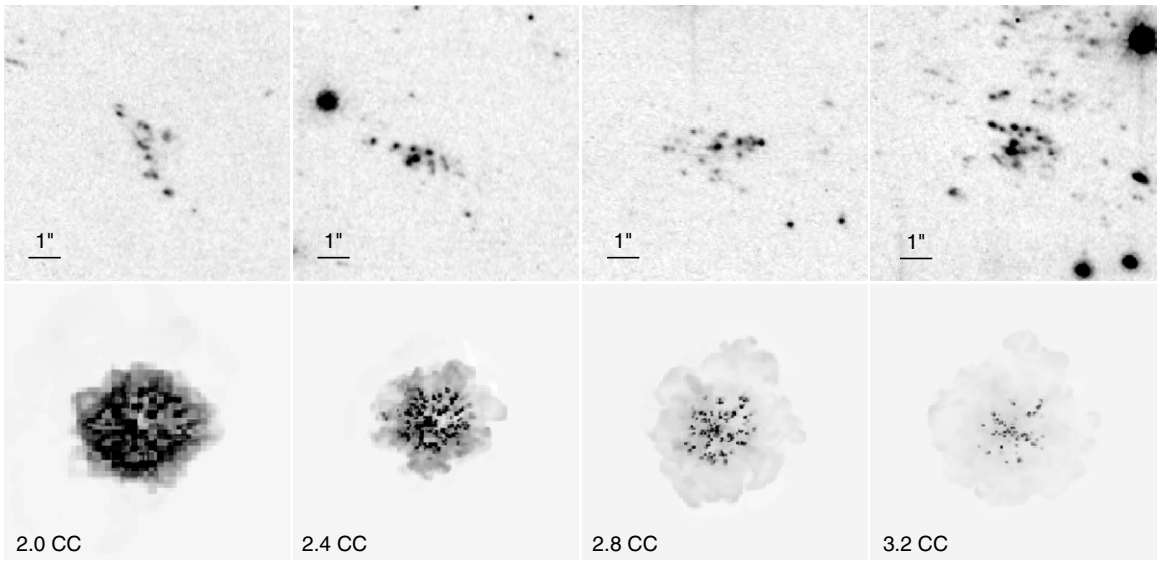

Figure 11. Top row: enlargements of the 2004 December ACS F675W + F775W image showing four ejecta knot clusters in the NE jet. Bottom Row: formation of knot clusters due to the fragmentation of a large ejecta clump after 2.0, 2.4, 2.8, and 3.2 cloud crushing times (Silvia et al. 2010).

1976) is of special interest for estimating lifetimes of ejecta fragments formed from the fragmentation of a larger knot. Although recently showing signs of fading, this group of ejecta knots has remained optically visible for nearly 60 yr, being easily detected on one of the first optical images taken of the remnant, namely a 1951 November Palomar 5 m plate (PH 563b; van den Bergh & Dodd 1970).

5. CONCLUSIONS

We report results of a survey on outlying debris knots around the young core-collapse SN remnant Cassiopeia A using *HST* images. These images reveal ejecta knot flickering, ablation emission tails, and knot fragmentation which are phenomena associated with the initial stages of the gradual merger of SN ejecta with, and the enrichment of, the surrounding ISM.

Our major findings and conclusions are as follows.

1. Substantial changes in the optical flux were seen in a significant percentage of the remnant's outer ejecta knots including the NE jet and eastern limb regions. In general, we detected no pattern in terms of brightness changes between three filters to suggest systematic changes in the line emissions between knot brightening or fading that might suggest a change of a knot's dominant ionization state.
2. A variety of light curves was found with some knots going up and down in brightness ("flickering") in times as short as nine months. Flux changes typically ranged from 50% to 800%. While large brightness changes were only seen in a minority of jet emission knots (<25%), smaller flux changes were apparent in a much larger percentage of knots approaching 50%.
3. The observed flickering of ejecta knots on times of months indicates knot scale lengths $\lesssim 10^{15}$ cm (i.e., $\lesssim 0\farcs02$) along with a highly inhomogeneous ISM or CSM. Knot interaction with small-scale CSM features is suggested by the rapid flickering of two eastern limb Knots, C and D (see Figure 6). In that case, the invisible CSM cloud or sheet which Knots C and D sequentially interacted with, leading to their sequential brightening, cannot be much larger than $0\farcs5$ or about 0.01 pc.
4. A small percentage (<5%) of knots were found to exhibit trailing emissions $0\farcs2$–$0\farcs7$ in length aligned along a knot's direction of motion suggestive of mass ablation tails due to high-velocity interaction with local CSM and ISM. These emission tails are bright relative to the knot suggestive of considerable ablated mass loss and could be either smooth or lumpy in intensity away from the knot's head. Because these linear knot + tail features are relatively short and brighter near the knot, they are unlike the linear emission "strings" seen in η Carinae.
5. We identified several tight clusters of ejecta knots which closely resemble fragmentation models for larger SN ejecta knots caused by a high-velocity interaction with a lower density ambient medium. Archival images of Cas A suggest that these knot clusters can survive and remain bright for several decades.

This work was supported by NASA through grants GO-8281, GO-9238, GO-9890, and GO-10286 from the Space Telescope Science Institute (STScI), which is operated by the Association of Universities for Research in Astronomy. J.M.S. acknowledges support at the University of Colorado through theoretical grants from STScI (AR-11774.01-A), NASA (NNX07-AG77G), and NSF (AST07-07474).

REFERENCES

Anderson, M. C., Jones, T. W., Rudnick, L., Drills, I. L., & Kang, H. 1994, ApJ, 421, L31
Arendt, R. G., Dwek, E., & Moseley, S. H. 1999, ApJ, 521, 234
Aschenbach, B., Egger, R., & Trumper, J. 1995, Nature, 373, 587
Bertin, E., & Arnouts, S. 1996, A&AS, 117, 393
Braun, R. 1987, A&A, 171, 233
Bykov, A. M. 2002, A&A, 390, 327
Chevalier, R. A. 1975, ApJ, 200, 698
Chevalier, R. A., & Kirshner, R. P. 1978, ApJ, 219, 931
Chevalier, R. A., & Kirshner, R. P. 1979, ApJ, 233, 154
Chevalier, R. A., & Oishi, J. 2003, ApJ, 593, L23
Cid-Fernandes, R., Plewa, T., Rózyczka, M., Franco, J., Terlevich, R., Tenorio-Tagle, G., & Miller, W. 1996, MNRAS, 283, 419
Currie, D. G. 2003, RevMexAA Conf. Ser., 15, 59
Douvion, T., Lagage, P. O., & Cesarsky, C. J. 1999, A&A, 352, L111

Dwek, E., & Arendt, R. 2007, in AIP Conf. Proc. 937, Supernovae 1987A 20 Years After: Supernovae and Gamma-Ray Bursters, ed. S. Immler, K. Weiler, & R. McCray (Melville, NY: AIP), 58
Elmhamdi, A., Danziger, I. J., Cappellaro, E., Della Valle, M., Gouiffes, C., Phillips, M. M., & Turatto, M. 2004, A&A, 426, 963
Fassia, A., Meikle, W. P. S., Geballe, T. R., Walton, N. A., Pollacco, D. L., Rutten, R. G. M., & Tinney, C. 1998, MNRAS, 299, 150
Fesen, R. A. 2001, ApJS, 133, 161
Fesen, R. A., & Gunderson, K. S. 1996, ApJ, 470, 967
Fesen, R. A., et al. 2001, AJ, 122, 2644
Fesen, R. A., et al. 2006a, ApJ, 636, 859
Fesen, R. A., et al. 2006b, ApJ, 646, 283
Filippenko, A. V., & Sargent, W. L. W. 1989, ApJ, 345, L43
Ford, H. C., et al. 1998, Proc. SPIE, 3356, 234
Hammer, N. J., Janka, H.-T., & Müller, E. 2010, ApJ, 714, 1371
Hammell, M. C., & Fesen, R. A. 2008, ApJS, 179, 195
Hamilton, A. J. S. 1985, ApJ, 291, 523
Hughes, J. P., Rakowski, C. E., Burrows, D. N., & Slane, P. O. 2000, ApJ, 528, L109
Hwang, U., & Laming, J. M. 2003, ApJ, 597, 362
Hwang, U., & Laming, J. M. 2009, ApJ, 703, 883
Hwang, U., et al. 2004, ApJ, 615, L117
Jones, T. W., Kang, H., & Tregillis, I. L. 1994, ApJ, 432, 194
Kamper, K., & van den Bergh, S. 1976, ApJS, 32, 351
Katsuda, S., & Tsunemi, H. 2006, ApJ, 642, 917
Kifonidis, K., Plewa, T., Janka, H.-T., & Müller, E. 2003, A&A, 408, 621
Kim, Y., Rieke, G. H., Krause, O., Misselt, K., Indebetouw, R., & Johnson, K. E. 2008, ApJ, 678, 287
Klein, R. I., McKee, C. F., & Colella, P. 1994, ApJ, 420, 213
Krause, O., Birkmann, S. M., Usuda, T., Hattori, T., Goto, M., Rieke, G. H., & Misselt, K. A. 2008, Science, 320, 1195
Krause, O., et al. 2005, Science, 308, 1604
Lagage, P. O., Claret, A., Ballet, J., Boulanger, F., Cesarsky, C. J., Cesarsky, D., Fransson, C., & Pollock, A. 1996, A&A, 315, L273
Mac Low, M.-M., McKee, C. F., Klein, R. I., Stone, J. M., & Norman, M. L. 1994, ApJ, 433, 757
Matheson, T., Filippenko, A. V., Ho, L. C., Barth, A. J., & Leonard, D. C. 2000, AJ, 120, 1499
Matteucci, F., & Greggio, L. 1986, A&A, 154, 279
Matteucci, F., Panagia, N., Pipino, A., Mannucci, F., Recchi, S., & Della Valle, M. 2006, MNRAS, 372, 265
Meaburn, J., Boumis, P., Walsh, J. R., Steffen, W., Holloway, A. J., Williams, R. J. R., & Bryce, M. 1996, MNRAS, 282, 1313
Meaburn, J., Wolstencroft, R. D., & Walsh, J. R. 1987, A&A, 181, 333
Mellema, G., Kurk, J. D., & Röttgering, H. J. A. 2002, A&A, 395, L13
Morse, J. A., Davidson, K., Bally, J., Ebbets, D., Balick, B., & Frank, A. 1998, AJ, 116, 2443
Morse, J. A., Fesen, R. A., Chevalier, R. A., Borkowski, K. J., Gerardy, C. L., Lawrence, S. S., & van den Bergh, S. 2004, ApJ, 614, 727
Müller, E., Fryxell, B., & Arnett, D. 1991, A&A, 251, 505
Nagasawa, M., Nakamura, T., & Miyama, S. M. 1988, PASJ, 40, 691
Norman, C., & Silk, J. 1979, ApJ, 228, 197
Pagel, B. E. J. 1997, in Nucleosynthesis and Chemical Evolution of Galaxies, ed. B. E. J. Pagel (Cambridge: Cambridge Univ. Press), 392
Pavlovsky, C., et al. 2004, ACS Instrument Handbook, Version 5.0 (Baltimore, MD: STScI)
Pittard, J. M., Falle, S. A. E. G., Hartquist, T. W., & Dyson, J. E. 2009, MNRAS, 394, 1351
Pittard, J. M., Hartquist, T. W., & Falle, S. A. E. G. 2010, MNRAS, 405, 821
Poludnenko, A. Y., Frank, A., & Mitran, S. 2004a, ApJ, 613, 387
Poludnenko, A. Y., et al. 2004b, ApJ, 604, 213
Raga, A. C., Esquivel, A., Riera, A., & Velázquez, P. F. 2007, ApJ, 668, 310
Redman, M. P., Meaburn, J., & Holloway, A. J. 2002, MNRAS, 332, 754
Reed, J. E., Hester, J. J., Fabian, A. C., & Winkler, P. F. 1995, ApJ, 440, 706
Rho, J., et al. 2008, ApJ, 673, 271
Scalo, J., & Elmegreen, B. G. 2004, ARA&A, 42, 275
Silvia, D. W., Smith, B. D., & Shull, J. M. 2010, ApJ, 715, 1575
Spyromilio, J. 1991, MNRAS, 253, 25P
Spyromilio, J. 1994, MNRAS, 266, L61
Stone, J. M., & Norman, M. L. 1992, ApJ, 390, L17
Strom, R., Johnston, H. M., Verbunt, F., & Aschenbach, B. 1995, Nature, 373, 590
Thorstensen, J. R., Fesen, R. A., & van den Bergh, S. 2001, AJ, 122, 297
Tsunemi, H., Miyata, E., & Aschenbach, B. 1999, PASJ, 51, 711
van den Bergh, S., & Dodd, W. W. 1970, ApJ, 162, 485
van den Bergh, S., & Kamper, K. W. 1983, ApJ, 268, 129
van den Bergh, S., & Kamper, K. W. 1985, ApJ, 293, 537
Wang, C.-Y., & Chevalier, R. A. 2002, ApJ, 574, 155
Weis, K., Duschl, W. J., & Chu, Y.-H. 1999, A&A, 349, 467
Willingale, R., Bleeker, J. A. M., van der Heyden, K. J., Kaastra, J. S., & Vink, J. 2002, A&A, 381, 1039
Woodward, P. R. 1976, ApJ, 207, 484
Young, P. A., et al. 2006, ApJ, 640, 891